THE JOURNAL OF PHYSICAL CHEMISTRY B

Article

pubs.acs.org/JPCB

Simultaneous Interfacial and Precipitated Supracrystals of Au Nanocrystals: Experiments and Simulations

Nicolas Goubet,[†,‡] Johannes Richardi,[†,‡] Pierre-Antoine Albouy,[§] and Marie-Paule Pileni*[,†,‡]

[†]Université Pierre et Marie Curie, UMR 7070, LM2N, 4 place Jussieu 75005 Paris, France

[‡]Centre National de la Recherche Scientifique, UMR 7070, LM2N, 4 place Jussieu 75005 Paris, France

[§]Laboratoire de Physique des Solides, Université Paris-Sud, 91405 Orsay, France

Supporting Information

ABSTRACT: Under solvent saturation, a precipitation of full-grown supracrystals on the one hand and the formation of well-defined supracrystalline films at the air−liquid interface on the other hand were previously observed for the first time (*J. Am. Chem. Soc.* **2012**, *134*, 3714−3719). Here, these two simultaneous growth processes are studied by additional experiments and by Brownian dynamics simulations. The thickness of the supracrystalline films and the concentration of free nanocrystals within the solution are measured as a function of the nanocrystal size. The simulations show that the first process of supracrystal growth is due to a homogeneous nucleation favored by solvent-mediated ligand interactions, while the second one is explained in terms of a diffusion process caused by a decrease in the surface energy when the particles penetrate the air−liquid interface. It is also verified that the presence of thiol molecules at the air−solution interface does not hinder the formation of supracrystalline films.

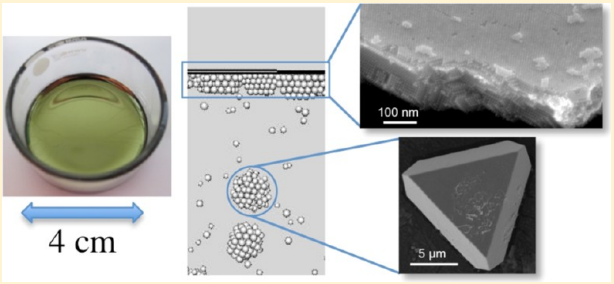

I. INTRODUCTION

Nanocrystals, used as building blocks, may self-assemble in long-range ordered assemblies so-called supracrystals. They are a good example of a meta-material, as their structural architectures induce collective properties and make them an emerging material.[1−3] In the past decades, most of these supracrystals were obtained by slow evaporation of a colloidal nanocrystal (NC) solution. Depending on the experimental conditions, two growth processes are observed:[4−7] either in solution (homogeneous nucleation)[8−11] or onto the substrate (heterogeneous nucleation).[12−15] The individual supracrystals obtained by homogeneous growth are characterized by well-defined shapes, whereas those grown by heterogeneous nucleation form thin films consisting of single-crystal domains sharing a common crystallographic axis normal to the substrate with an in-plane random orientation. Other ways to grow supracrystals were developed, for example, a water−air interface may be used to obtain a 2D[16,17] or 3D superlattice as supracrystals with perfectly faceted hexagonal shapes.[18] Recently,[5,6] it was demonstrated by experiments and simulations in the case of gold supracrystals that the solvent used to disperse NCs before deposition is one of the key parameters which determines the growth mechanism.

We previously demonstrated, by experiments, simultaneous growth of two types of supracrystals made of Au NCs without evaporation.[19] Due to the confinement, the gas phase saturates with the solvent and the evaporation process is stopped, allowing crystallization for several days. The resulting supracrystals show two different morphologies: films on the toluene−air interface and polyhedral crystal formed in the bulk solution. To better understand both growth processes, the experimental results are revisited and additional measurements such as the supracrystal thickness and the degree of free NCs within the solution are carried out. Then, a theoretical interaction model taking into account the particle−particle and particle−interface interactions is developed. This model is used in Brownian dynamics simulations to verify if it is able to reproduce the experimental observations.

2. EXPERIMENTAL AND THEORETICAL METHODS

2.1. Products and Characterization Methods. All products and solvents were purchased from a variety of sources and used without purification. Toluene was procured from Riedel de Haën (>98%) and ethanol (99.8%) from Prolabo. Chlorotriphenylphosphine gold(I) (98%) and *tert*-butylamine borane complex (>97%) were from STREM. 1-Dodecanethiol and boran−ammonia complex (97%) were from Aldrich.

Transmission electron microscopy (TEM) and scanning electron microscopy (SEM) with low and high resolution images were obtained with JEOL JEM 1011, JEOL JSM-5510LV, and Hitachi SU-70 instruments respectively. The grazing incidence small angle scattering (GISAXS) patterns are

Special Issue: Paul F. Barbara Memorial Issue

Received: August 30, 2012
Revised: October 19, 2012
Published: October 19, 2012

   dx.doi.org/10.1021/jp308608g | *J. Phys. Chem. B* 2013, 117, 4510−4516

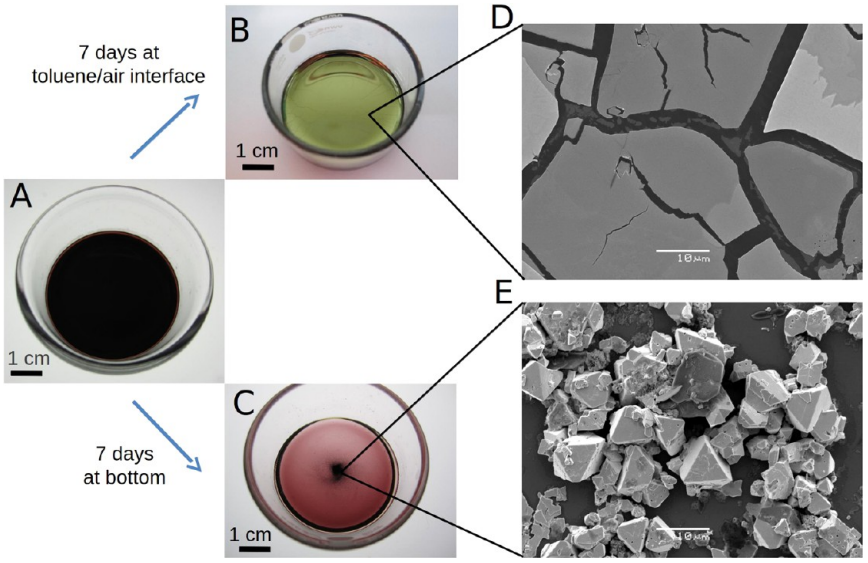

Figure 1. Upside view of the colloidal solution at initial state (A), the supracrystal deposition at the air−toluene interface after 7 days (B), and the supracrystal precipitated at the bottom of the beaker after removing the interfacial deposition (C). SEM pictures of the interfacial film (D) and the simultaneous precipitate (E).

acquired with a homemade system. The X-ray generator is a rotating copper anode operated with a small-size focus (0.1 × 0.1 mm^2) at 40 kV and 20 mA. The optics consists of two parabolic multilayer-graded mirrors in K−B geometry.

2.2. Syntheses of Au NCs. The synthesis of Au NCs with various sizes (from 4 to 8 nm) was reported in a previous paper.[5] Two solutions are used (for simplicity called A and B) to produce Au NCs. Solution A consists of 0.25 mmol of chlorotriphenylphosphine Au(I) dissolved in 25 mL of toluene to which 500 μL of dodecanthiol is added. Solution B is made of 2.5 mmol of *tert*-butylamine borane complex in 15 mL of toluene. Changing the amount of dodecanethiol in A and reducing power in B controls the size of NCs. At the end of the synthesis, Au NCs are dispersed in toluene. One drop of the colloidal solution is deposited on an amorphous carbon-coated copper grid placed on an absorbent paper. Figure S1A (Supporting Information) shows the bright field TEM images of Au NCs with a low size distribution (Figure S1B, Supporting Information) and with different sizes noted.

2.3. Simultaneous Supracrystallization. The simultaneous supracrystallization was described in our previous paper.[19] Briefly, the colloidal solution is kept in a closed container, and after 7 days, for the favorable NC sizes, a bright thin interfacial film and precipitates appear. The interfacial supracrystals can be collected with a ringlike DuNouy ring, and precipitated supracrystals are withdrawn from the bottom of the beaker. The supracrystal deposited on a substrate (Si or HOPG) can be probed by GISAXS to determine the corresponding distance between NCs (see the Supporting Information).

2.4. Simulation Method. The assembly of Au NCs dispersed in solution is modeled at a NC level by Brownian dynamics.[20,21] In previous simulations,[5,6] the evaporation of Au NCs was studied neglecting any possible attraction between NC and the air−solution interface. Here, we propose an improved model for the interactions between NCs and the air−toluene interface.

The interaction potential between the NCs is the same as the one used in previous simulations.[5,6] It is defined as a sum of three terms:[5,6,22] the van der Waals attraction between the metallic cores of the particles, the free energy of mixing of the thiol ligands, and the elastic compression of the ligands. The interaction terms and parameters were given in our previous paper.[5] In this article, two ways to calculate the effective Hamaker constant for the van der Waals attraction between the metallic NCs were proposed and it has been shown that its influence on the simulation results is small. Here, a value of 1.95 eV is used.

The interaction between the NCs and the air−toluene interface is modeled by using two approaches. The first one is based on the change in surface energy due to the NC penetration of the air−toluene interface, whereas the second one takes into account the presence of some free ligands at the interface.

In the first model, the change in the surface energy is expressed as follows:[20]

$$u_{surf}(r) = 2\pi\sigma_l R(R - r) - \pi\sigma_s(R^2 - r^2) \quad (1)$$

where r, R, σ_l, and σ_s are the distance between the center of the NC and the air−toluene interface, the particle radius (including the coating layer of 1.78 Å), and the air−coating and air−toluene surface tensions, respectively. The first term in eq 1 corresponds to the energy due to the interface between the NC coating and the gas phase, whereas the second term is caused by the decrease in the toluene−air interface due to the penetration of the interface by the NC. The surface energy of dodecane ($\sigma_l = 25.4 \times 10^{-3}$ J m^{-2}) is used for the coating, since the thiol group is attached to the NCs. Therefore, the thiol group is quite far from the interface and is expected to play no significant role in the interaction between air and the coating molecules. Atomistic simulations have shown that the interactions between NCs and interfaces are well described by approaches using the interfacial energy.[23,24] The energy change due to the disappearance of the interface between ligand and solvent is neglected in our approach. To verify this approximation, we have estimated the solvent−ligand interfacial tension from the Dupré equation which can be written as $\sigma_{ls} = \sigma_{ss} + \sigma_{ll} - 2(\sigma_{ss}\sigma_{ll})^{1/2}$, where σ_{ls}, σ_{ss}, and σ_{ll} are the interfacial

dx.doi.org/10.1021/jp308608g | J. Phys. Chem. B 2013, 117, 4510−4516

tensions between ligand and solvent and the surface tensions of the solvent and the ligand, respectively. For dodecane as ligand and toluene as solvent, we obtain a value of 0.084 mJ m^{-2} for σ_{sl}, which shows that the energy change due to the ligand–solvent interface can be neglected in this case. In the case of hexane, σ_{sl} is larger (0.64 mJ m^{-2}), but even including this term in the model leads to a purely repulsive potential. These calculations show that the particle–interface interaction potential is not markedly influenced by the decrease of the ligand–solvent interface.

Under the experimental conditions, the presence of free ligand in the solution cannot be excluded. To study the influence of free ligand molecules at the interface, we calculate the interaction between a NC and a monolayer of thiols at the air–toluene interface. It may be modeled as a sum of the free energy of mixing of the thiol ligands and the elastic compression of the ligands:

$$u_{surfn}(r) = u_{surf,mix}(r) + u_{surf,elastic}(r) \quad (2)$$

It corresponds to the interaction between a curved surface and a planar wall, where both are made of ligand molecules. Using the Derjarguin approximation,[25] the equations for the energy terms were obtained from the formula given in the literature for the interaction between two planar walls made of ligands.[26,27] The equations obtained by this way are given in the Appendix.

Brownian dynamics simulations were carried out by integration of the Langevin equations using an algorithm proposed by Allen.[28] At the top of the simulation box, there is the air–liquid interface described by interaction potential 1 or 2, while a wall at the bottom represents the substrate.[20] Details of the simulations are presented elsewhere.[5] For the simulations, the number of particles is 10 000.

The formation of clusters during the simulation is studied by snapshots, which show the positions of the particles in the simulation box. The structures in the snapshots can be directly compared to SEM images obtained after evaporation of the nanoparticle solutions.

3. RESULTS AND DISCUSSION

Colloidal solutions (Figure 1A), with different NCs focused sizes (5–8 nm) (Figure S1, Supporting Information) and narrow size distribution (<10%) are used to build 3D NCs arrays. The NCs are dispersed in toluene. After 1 week without evaporation of the solvent, colloidal solutions exhibit a Au mirror on the toluene–air interface (Figure 1B) and a precipitate at the bottom of the beaker (Figure 1C). This phenomenon is due to two simultaneous supracrystal growth processes leading to two different morphologies.[19] The first one results in a precipitate of full-grown polyhedrons making a supracrystalline powder visible at the bottom of the beaker in Figures 1C,E and 2C. The resulting face centered cubic (fcc) (Figure 2C) supracrystals display well-defined micrometric shapes. In Figure 3, we can see that the black powder (i.e., supracrystals) does not grow on the glass wall but is sedimented at the bottom of the cell. This observation confirms a homogeneous growth of the supracrystal. The second one grows on the air–toluene interface visible as a mirror in Figure 1B,D. As the interface area is evaluated to 12.6 cm^2, this interfacial growth results in supracrystalline films on a macroscopic range. The GISAXS show that the films crystallize in the face centered cubic system (fcc) and display a [111] supracrystalline orientation (Figure 2). In the case of NCs with 5 nm diameter, their corresponding interfacial films exhibit a mixture between fcc and bcc crystalline structures oriented along [111] and [110], respectively (Figure 2).

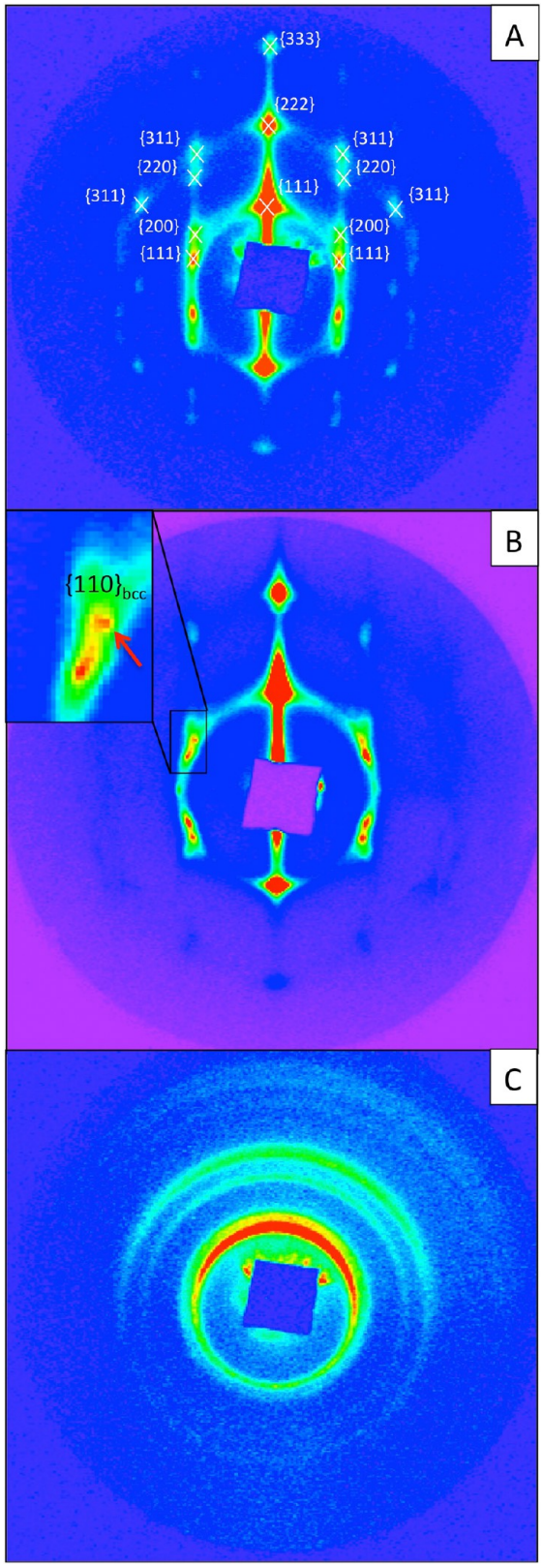

Figure 2. Typical SAXS pattern of interfacial supracrystal made with 6 nm (A), 5 nm (B), and precipitated supracrystal made with 6 nm (C).

dx.doi.org/10.1021/jp308608g | J. Phys. Chem. B 2013, 117, 4510–4516

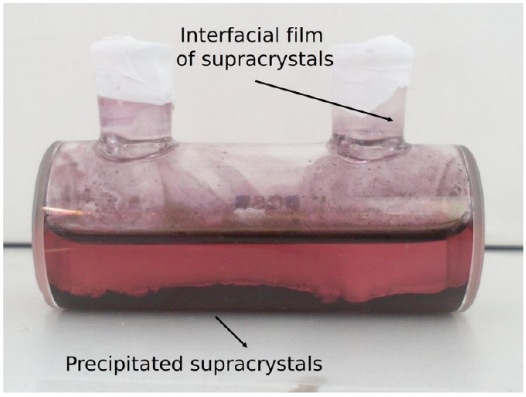

Figure 3. Colloidal solution after 7 days in a curved wall cell.

The amount of NCs remaining in solution is estimated by extracting a few μL of solution from the overall system after 7 days and by recording its surface plasmon resonance (SPR) spectrum. Using the usual beaker with an interface area of 12.6 cm^2, the amount of remaining NCs is 100% (no precipitation), 51%, 13%, 5%, and 4% for 4, 5, 6, 7, and 8 nm, respectively. By replacing the initial beaker by one with a toluene−air area of 0.2 cm^2, the percentage in NCs remaining in solution markedly increases and is 100, 88, 34, 14, and 13%, respectively. This clearly shows that the amount of NCs remaining in solution markedly depends on the air−toluene interface area. The thickness of interfacial films is deduced by tilting the sample (Figure 4). For any NC size and 10^{-2} M as the initial Au NC concentration, the film thickness (Figure 4A) remains in the same order of magnitude (200−300 nm). On decreasing the initial Au concentration, the thickness of the interfacial film progressively drops (Figure 4A−C): A decrease of a factor of 10 of the initial Au NC concentration (from [Au] = 10^{-2} M to [Au] = 10^{-3} M) induces a drop of the interfacial thickness by a similar factor with an average thickness of 30−45 nm (Figure 4C,D). This clearly shows that the thickness of the interfacial supracrystals is controlled by the initial concentration of Au NCs, while the size dependent van der Waals interaction between NCs is not a key parameter in the interfacial film formation. This thickness control is important for the future application of NC supracrystal films.

The supracrystals (interface and precipitated) are dissolved in hexane with formation of a highly stable colloidal solution. By depositing a drop of the colloidal solution on a grid, the TEM images and the corresponding histogram perfectly agree with those corresponding to the NCs remaining in solution, as shown in Figure 5. This clearly rules out a segregation process with the larger NCs involved in the formation of supracrystals and the smaller remaining in the solution. Furthermore, in hexane, the Au NCs remain in solution without any supracrystal growth as observed with toluene.

The supracrystal growth mechanisms are now modeled at a particle level by the Brownian dynamics simulations. As shown in our previous work,[5,6] the interaction potential between the NCs is attractive for toluene and repulsive for hexane. The attractive peak in toluene increases with the NC diameter. The interaction between the NCs and the air−solution interface calculated from eq 1 is shown in Figure 6A. For toluene, the total surface energy is decreased due to the lower surface energy of the NC coating ($\sigma_l = 25.4 \times 10^{-3}$ J m^{-2}) compared to the one of the air−toluene ($\sigma_s = 28.4 \times 10^{-3}$ J m^{-2}). The strength and range of the attraction by the interface increase with the particle diameter. Please note that the particle−interface interaction (not shown here) is purely repulsive in the case of hexane ($\sigma_s = 24.0 \times 10^{-3}$ J m^{-2}).

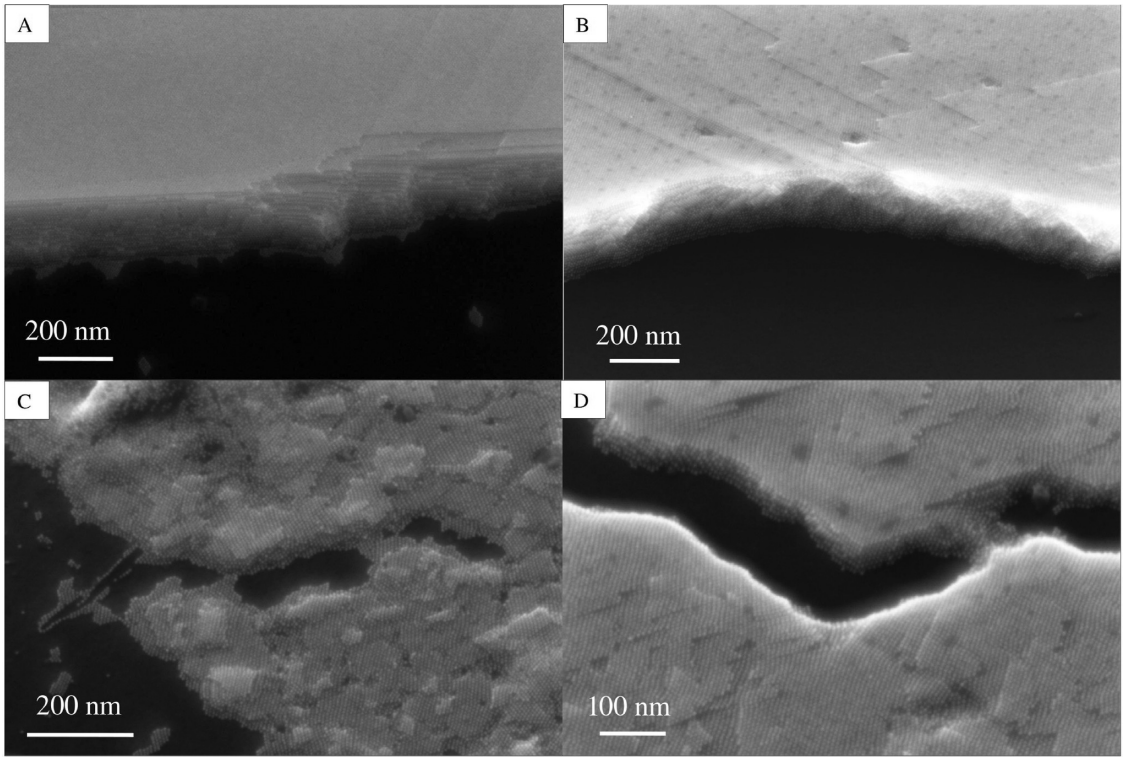

Figure 4. Tilted configurations of interfacial supracrystal made with a colloidal solution at 10^{-2} M (A), 5.10^{-3} M (B), and 10^{-3} M (C, D).

dx.doi.org/10.1021/jp308608g | J. Phys. Chem. B 2013, 117, 4510−4516

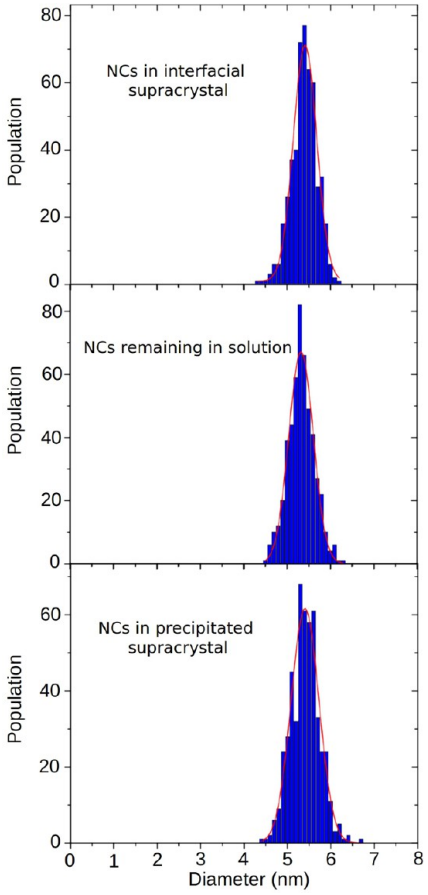

Figure 5. Sample of supracrystal made of 5 nm NCs redispersed in hexane. Size distribution of NCs constituting the interfacial supracrystal (A), the remaining colloidal solution (B), and the precipitated supracrystal (C).

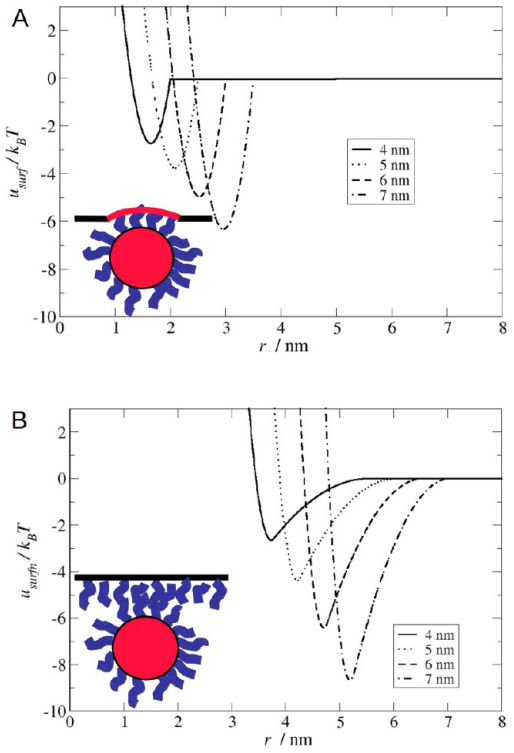

Figure 6. Energy evolution of a Au NC crossing the air−toluene interface in toluene as predicted by eq 1 (A). Energy evolution of Au NC approaching a monolayer of ligands at the air−toluene interface as predicted by eq 2 (B).

Taking into account these interaction potentials, the supracrystal growths at the air−toluene interface and in solution are simulated. The theoretical description of the growth of supracrystals experimentally observed leads to problems related to the very low concentrations (reduced density: 5×10^{-10}) and to the period of several days. Thus, when simulations are carried out at the experimental concentrations, no supracrystals during the small time of several microseconds are accessible simply due to the fact that the particles have not even the time to meet each other. To cope with this problem, simulations are carried out at volume fractions varying from 0.001 to 0.1. It is observed that the qualitative results do not depend on the volume fractions. However, it must be emphasized that simulations only show the initial phase of supracrystal formation, which explains the small size of aggregates observed with respect to the experiments. Figure 7 shows typical snapshots of the final configurations obtained at a volume fraction of 0.005. For NC diameters larger than 4 nm (from Figures 7B−D), supracrystals form within the solution by homogeneous nucleation. This is due to the attraction between the NC cores predicted by the potentials between the NCs and has been previously observed in simulations.[5] In parallel, a new layer-by-layer growth of supracrystals is observed at the air−toluene interface. This kind of flat supracrystals sticking to the interface is absent at the bottom of the simulation box representing the substrate. Note that for a NC diameter of 4 nm in toluene (Figure 7A,E) and at any NC size in hexane, supracrystal formation is absent within the solution and at the air−liquid interface.

In the previous simulations, it is assumed that only particles may adsorb at the air−toluene interface. However, the presence of free ligands cannot be ruled out. To study the influence of ligands at the interface, we calculate the interaction between a NC and a monolayer of thiols adsorbed at the air−toluene interface from eq 2. Figure 6B shows the evolution of the energy of the NCs approaching the air−toluene interface. Due to the energy of mixing, an attractive peak is obtained that increases with increasing NC diameter. It is surprising that both models starting from very different hypotheses predict the same behavior in almost a quantitative way. Simulations are carried out with this model. Parts E−H of Figure 7 show typical snapshots of the final configurations obtained at a volume fraction of 0.005. The results are very similar to those obtained with the first model (Figure 7A−D). Both approaches predict two growth mechanisms, one within the solution and the other at the air−liquid interface only for NC diameters equal or larger than 5 nm in toluene as observed in the experiments. Please note that additional calculations have shown that in hexane the NC−interface potentials obtained from both eqs 1 and 2 are purely repulsive and no supracrystal growth is observed in accord with the experiment.

From the good agreement between experiments and simulations, the formation of the NC film at the air−toluene interface is explained as follows: Due to the attractive potential between NCs and the interface, NCs are trapped at the solution surface and form monolayers. The attraction between NCs in toluene leads to a further growth on this first layer. Once the surface is covered by a Au NC monolayer, further adsorption of NCs is governed by the diffusion of the NCs or aggregates to

dx.doi.org/10.1021/jp308608g | J. Phys. Chem. B 2013, 117, 4510−4516

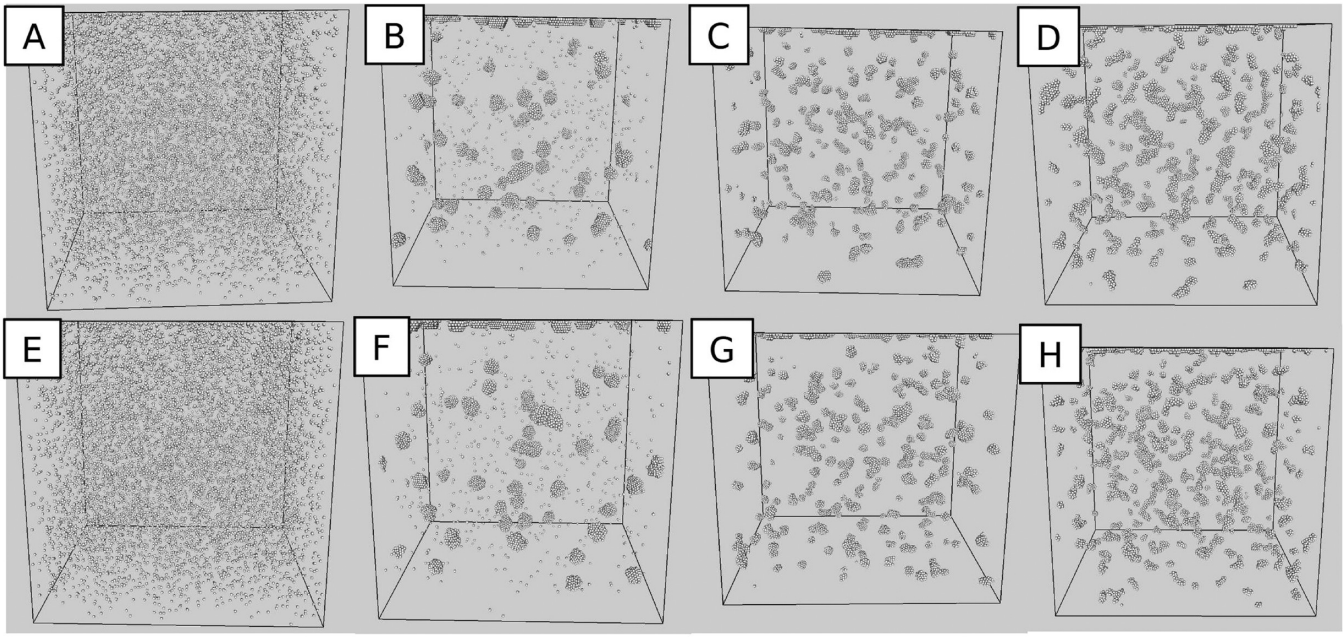

Figure 7. Brownian dynamics simulation results of the Au NC assembly close to the air−toluene interface: Snapshots of the final configurations for NCs with various diameters dispersed in toluene. The first (A−D) and second (E−H) rows show results for simulations carried out using eqs 1 and 2, respectively, for the NC−interface interaction.

the air−toluene interface. This explains why the film thickness becomes thinner with decreasing initial concentration of NCs. Some solvent stays within the NC film. Only when this film is deposited on a substrate, the rest of the solvents evaporate, leading to the formation of cracks and dislocation. In fact, during such a drying process, small defects within the film lead to dislocations that reduce the final mechanical stability of the films. In contrast to the precipitated supracrystals, no dislocations appear.

For any NC sizes except Au_5, the interfacial and precipitated supracrystals exhibit an fcc structure (Figure 2). In the case of Au_5 interfacial films, the coexistence of fcc and bcc structures is observed. However, the simulations shown above usually give compact structures with a random sequence of hexagonal layers. The absence of bcc structures may be explained by the fact that the formation of noncompact structures is due to specific many body interactions which are not taken into account in our simulation model.[29−31] To study the stability of the compact (hcp/fcc) or bcc structures with respect to the NC size and the interparticle distance, we propose to use the following criterion from the literature[29] based on the interaction of the ligands between the NCs. Landman and Luedtke[29] have proposed that the formation of bcc structures is observed instead of fcc ones, when the ligands between the second nearest neighbors are in contact within the bcc lattice. This leads to the criterion for the appearance of bcc structures: $L > {}^1/_2(D_{nnn} - d)$, where L, d, and D_{nnn} are the length of the alkyl chain, the NC diameter, and the second nearest distance between NCs in this lattice, respectively. D_{nnn} is calculated from the distance D between NC centers using the equation $D_{nnn} = 2/\sqrt{3}D$. Note that this assumption was confirmed by atomistic simulations.[29] The values of ${}^1/_2(D_{nnn} - d)$ were calculated for each sample of supracrystals and are given in Table 1. For the interfacial and precipitated supracrystals of Au_5, values between 1.6 and 1.7 nm are obtained. Since L is equal to 1.78 nm here, the bcc structure can be expected to be more stable for these samples. For the other NC diameters, the calculated ${}^1/_2(D_{nnn} - d)$ are larger than the ligand length predicting the formation of fcc structures. The fact that bcc structures are observed only in the interfacial supracrystals whereas only fcc supracrystals are produced in the precipitated supracrystals may be explained as follows: The interfacial supracrystal film floats at the air−toluene interface, and some solvent molecules remain in the alkyl chain interstices, favoring a lesser compact stacking. Conversely, expelling solvent molecules from the alkyl chain during the crystal growth produces the precipitated supracrystals. For NC sizes larger than 5 nm, both criteria predict fcc structures in agreement with the experiment.

Table 1. The Criterion for the Appearance of bcc Structures, ${}^1/_2(D_{nnn} - d)$ (See Text)

		Au_5	Au_6	Au_7	Au_8
${}^1/_2(D_{nnn} - d)$ (nm)	interfacial supracrystals	1.7	1.8	1.8	1.8
	precipited supracrystals	1.6	1.9	2.1	2.1

CONCLUSION

Here additional experiments show that the thickness of the interfacial film observed at the interface does not depend on the NC size but on its concentration. The presence of NCs within the solution markedly decreases with increasing NC size. In good agreement with the experiments, two growth processes are observed in the simulations using confined conditions only for Au NCs with sizes from 5 to 8 nm in toluene that disappear for smaller NCs. Furthermore, simulations and experiments show that these growth processes do not take place when hexane is used as solvent to disperse the NCs. The growth processes are explained in terms of an increase in the NC−NC attraction and change in surface energy due to the NC penetration of the air−toluene interface that is repulsive in hexane. The NC adsorption on the interface can be assumed as a formation of Gibbs monolayer. With 5 nm Au NCs, the presence of both fcc/bcc structures is again explained in terms

dx.doi.org/10.1021/jp308608g | J. Phys. Chem. B 2013, 117, 4510−4516

of a specific criterion related to many-body interactions. This interfacial growth is a novel way to build up well-oriented supracrystalline films on a macroscopic scale. Note that this interfacial crystal growth is also observed in Nature. In cave pools, which contains carbonate supersaturated water, calcite or aragonite can crystallize and float at the air−water interface.[32] In both cases, the air−liquid interface is quite perfect, leading to very homogeneous interfacial supracrystals.

APPENDIX

For the free energy of mixing of the thiol ligands, three different regimes must be distinguished:

(i) The first regime is defined by an interface−NC separation $r > R + 2L$, where L is the length of the alkyl chain. The free energy of mixing of the ligands can be neglected, since the ligand layers do not overlap. Here, R is defined as the particle radius without the ligand shell.

(ii) The second regime is defined as $R + L < r < R + 2L$. The free energy of mixing corresponds to

$$\frac{u_{\mathrm{surf,mix,1}}(r)}{kT} = \frac{\pi d}{V_s}\phi_{\mathrm{av}}^{\ 2}\left(\frac{1}{2} - \chi\right)[r - (d + 2L)]^2 \qquad \text{(A1)}$$

where V_s, ϕ_{av}, and χ are the volume of the solvent molecule, the volume fraction of the ligand segments in the thiol shell, and the Flory parameter, respectively. We assume that the volume fraction ϕ_{av} of the ligand segments in the thiol shell corresponds to dense packing.

(iii) The third regime is defined as $R < r < R + L$. The free energy of mixing is given by

$$\frac{u_{\mathrm{surf,mix,2}}(r)}{k_{\mathrm{B}}T} = 2\frac{\pi d}{V_s}\phi_{\mathrm{av}}^{\ 2}\left(\frac{1}{2} - \chi\right)L^2\left[3\ln\left(\frac{L}{r-d}\right) + 2\left(\frac{r-d}{L}\right) - \frac{3}{2}\right] \qquad \text{(A2)}$$

The elastic contribution due to the ligand compression, $u_{\mathrm{elastic}}(r)$, is neglected for particle separations $r > R + L$. At closer contact $r < R + L$, the chain is compressed by the presence of the NC core. The following equation is obtained:

$$\frac{u_{\mathrm{surf,elastic}}(r)}{kT} = 2\pi\nu d\left[(r-d)\left(\ln\frac{r-d}{L} - 1\right) + L\right] \qquad \text{(A3)}$$

where ν is the number of ligands per unit area of the NC.

The calculations of the parameters V_s, ϕ_{av}, χ, and ν have been explained in detail in the previous paper.[5]

ASSOCIATED CONTENT

Supporting Information

TEM pictures of Au_8, Au_7, Au_6, Au_5, and Au_4 and their diameter distribution and internanocrystal distance determination. This material is available free of charge via the Internet at http://pubs.acs.org.

AUTHOR INFORMATION

Corresponding Author

*E-mail: marie-paule.pileni@upmc.fr.

Notes

The authors declare no competing financial interest.

ACKNOWLEDGMENTS

M.-P.P. has received funding from Advanced Grant of the European Research Council under Grant Agreement No. 267129.

REFERENCES

(1) Eichenfield, M.; Chan, J.; Camacho, R. M.; Vahala, K. J.; Painter, O. *Nature* **2009**, *462*, 78−82.
(2) Thomas, E. L.; Gorishnyy, T.; Maldovan, M. *Nat. Mater.* **2006**, *5*, 773−774.
(3) Pileni, M. P. *Acc. Chem. Res.* **2008**, *41*, 1799−1809.
(4) Prasad, B. L. V.; Sorensen, C. M.; Klabunde, K. J. *Chem. Soc. Rev.* **2008**, *37*, 1871−1883.
(5) Goubet, N.; Richardi, J.; Albouy, P.-A.; Pileni, M.-P. *Adv. Funct. Mater.* **2011**, *21*, 2693−2704.
(6) Goubet, N.; Richardi, J.; Albouy, P. A.; Pileni, M. P. *J. Phys. Chem. Lett.* **2011**, 417−422.
(7) Motte, L.; Billoudet, F.; Lacaze, E.; Douin, J.; Pileni, M. P. *J. Phys. Chem. B* **1997**, *101*, 138−144.
(8) Abecassis, B.; Testard, F.; Spalla, O. *Phys. Rev. Lett.* **2008**, *100*, 115504.
(9) Compton, O. C.; Osterloh, F. E. *J. Am. Chem. Soc.* **2007**, *129*, 7793−7798.
(10) Talapin, D. V.; Shevchenko, E. V.; Kornowski, A.; Gaponik, N.; Haase, M.; Rogach, A. L.; Weller, H. *Adv. Mater.* **2001**, *13*, 1868−1871.
(11) Rupich, S. M.; Shevchenko, E. V.; Bodnarchuk, M. I.; Lee, B.; Talapin, D. V. *J. Am. Chem. Soc.* **2010**, *132*, 289−296.
(12) Sigman, M. B.; Saunders, A. E.; Korgel, B. A. *Langmuir* **2003**, *20*, 978−983.
(13) Courty, A.; Fermon, C.; Pileni, M. P. *Adv. Mater.* **2001**, *13*, 254−258.
(14) Lisiecki, I.; Albouy, P. A.; Pileni, M. P. *Adv. Mater.* **2003**, *15*, 712−716.
(15) Bian, K.; Choi, J. J.; Kaushik, A.; Clancy, P.; Smilgies, D.-M.; Hanrath, T. *ACS Nano* **2011**, *5*, 2815−2823.
(16) Bigioni, T. P.; Lin, X.-M.; Nguyen, T. T.; Corwin, E. I.; Witten, T. A.; Jaeger, H. M. *Nat. Mater.* **2006**, *5*, 265−270.
(17) Campolongo, M. J.; Tan, S. J.; Smilgies, D.-M.; Zhao, M.; Chen, Y.; Xhangolli, I.; Cheng, W.; Luo, D. *ACS Nano* **2011**, *5*, 7978−7985.
(18) Wang, S.; Sato, S.; Kimura, K. *Chem. Mater.* **2003**, *15*, 2445−2448.
(19) Goubet, N.; Portalès, H.; Yan, C.; Arfaoui, I.; Albouy, P.-A.; Mermet, A.; Pileni, M.-P. *J. Am. Chem. Soc.* **2012**, *134*, 3714−3719.
(20) Lalatonne, Y.; Richardi, J.; Pileni, M. P. *Nat. Mater.* **2004**, *3*, 121−125.
(21) Allen, M.; Tildesley, D. *Computer simulation of liquids*; Clarendon Press: Oxford, 1993.
(22) Khan, S. J.; Pierce, F.; Sorensen, C. M.; Chakrabarti, A. *Langmuir* **2009**, *25*, 13861−13868.
(23) Fan, H.; Resasco, D. E.; Striolo, A. *Langmuir* **2011**, *27*, 5264−5274.
(24) Luo, M.; Mazyar, O. A.; Zhu, Q.; Vaughn, M. W.; Hase, W. L.; Dai, L. L. *Langmuir* **2006**, *22*, 6385−6390.
(25) Hunter, R. J. Oxford University Press: Oxford, 2001.
(26) Smitham, J. B.; Evans, R.; Napper, D. H. *J. Chem. Soc., Faraday Trans. 1* **1975**, *71*, 285−297.
(27) Evans, R.; Smitham, J. B.; Napper, D. H. *Colloid Polym. Sci.* **1977**, *255*, 161−167.
(28) Allen, M. P. *Mol. Phys.* **1980**, *40*, 1073−1087.
(29) Landman, U.; Luedtke, W. D. *Faraday Discuss.* **2004**, *125*, 1−22.
(30) Courty, A.; Richardi, J.; Albouy, P.-A.; Pileni, M.-P. *Chem. Mater.* **2011**, *23*, 4186−4192.
(31) Korgel, B. A.; Fitzmaurice, D. *Phys. Rev. B* **1999**, *59*, 14191.
(32) Taylor, P. M.; Chafetz, H. S. *J. Sediment. Res.* **2004**, *74*, 328−341.